A Numerical Approach to Study Shell-Side Fluid Flow in Shell-and-Tube Heat Exchangers

A Numerical Approach to Study Shell-Side Fluid Flow in Shell-and-Tube Heat Exchangers

A. Quartararo[1], P.A. Di Maio[1], I. Moscato[2] E. Vallone[1], G. Guagliardo[1]

[1]Department of Engineering, University of Palermo, Viale delle Scienze, Ed. 6, 90128 Palermo, Italy
[2]Fusion Technology Department – Programme Management Unit, EUROfusion Consortium, Boltzmannstraße 2, 85748 Garching, Germany

Corresponding author's e-mail: andrea.quartararo@unipa.it

Abstract. The detailed CFD simulation of the shell-side flow inside shell-and-tube heat exchangers results prohibitive for large-size components, due to the large number of tubes, together with the multi-scale nature of the flow features. To overcome this issue, the porous media approach can be adopted, substituting the tube bundle with a porous domain, where a suitable momentum sink term in the Navier-Stokes equation is provided. In this paper, a novel numerical approach to estimate the crossflow shell-side pressure drop is presented: a complete characterization of the tube bundle was performed by running 2D-CFD steady-state isothermal analyses, collecting pressure gradient magnitudes and directions for different mass flow rates and angles of attack of the incoming flow. The approach was validated against numerical results and compared to the methodologies currently available. Models, assumptions, and boundary conditions are herewith reported and thoroughly discussed, alongside the main results obtained.

1. Introduction

Shell-and-tube Heat eXChangers (HXC) are the most widely used HXCs in process industries, power plants, petroleum refinery and chemical industries. This technology draws its great diffusion from the fairly large ratios of heat transfer area to volume and weight, the easy manufacturability and maintainability and the flexibility to meet a wide range of pressures, temperatures and mass flow rates, as well as the possibility to work with phase-changing and severely fouling and corrosive fluids [1]. The design of shell-and-tube HXCs is based on reliable and well-consolidated methodologies, mainly grounded on experimental data [2]. In fact, a large number of tubes, together with the multi-scale nature of the flow features inside the shell-and-tube HXCs, pose an obstacle to the development of detailed numerical-based methodologies, capable to reproduce the details of the flow field without the need to perform unduly geometrical simplifications.

In fact, despite the great increase of Computational Fluid Dynamics (CFD) codes capabilities, driven by the widespread availability of powerful computing resources, the detailed simulation of large HXCs, generally equipped with several thousand tubes, still results prohibitive. As a consequence, most of the recent research activity on HXCs involving detailed CFD simulations is focussed on small-size equipment [3, 4, 5]. Nevertheless, the level of detail achievable with these simulations allows to gain a deep understanding of the underlying physical processes, and

it is of great value to check the occurrence of bypass and recirculation phenomena, responsible for an efficiency reduction of the HXCs.

To overcome this issue, the *porous media concept*, also referred to as *distributed resistance approach*, was firstly introduced by Patankar and Spalding [6], and further developed by other authors [7, 8, 9]. The idea behind this approach is to treat the tube bundle as a porous medium, adopting a modelling technique that correctly reproduces the interaction between fluid and tubes, by means of suitable source terms in the Navier-Stokes equations. The closure problem thus requires additional equations (usually experimental correlations) that relate pressure losses and heat transfer coefficient with the local field variables of the fluid. With regard to pressure loss, it can be obtained by adopting suitable friction factors and geometrical parameters to consider both the bundle porosity and its permeability.

It is moreover important to remark that the friction factor depends on both the shell-side fluid velocity magnitude and its direction. Nevertheless, while the distinction between cross and parallel-flow is always considered within this approach, the friction factor is usually assumed to be independent on the cross-flow angle [7, 10] or calculated separately along the two orthogonal HXC main directions [9].

In this paper, a different implementation of the porous medium approach is proposed: to provide a reliable estimate of the friction factor, an elementary cell of the tube bundle, namely *test bundle*, was simulated by means of 2D-CFD steady-state analyses, following a numerical technique based on the Finite Volume Method (FVM) and adopting the commercial CFD code ANSYS CFX 2020 R2 [11]. The test bundle simulations allowed to obtain a map of pressure gradient magnitudes and directions for different mass flow rates and angles of attack of the incoming flow, and the data acquired were used to define a cross-flow friction factor dependent on the local main flow direction.

To validate this novel approach, a complete 2D-CFD simulation of the inlet section of a large shell-and-tube HXC was performed, with a sufficient level of detail able to capture the flow field around more than 1200 tubes. Furthermore, the same geometry was simulated adopting the porous media approach in ANSYS CFX. The momentum sink term was defined both according to the formulation given in [10] and implementing the data obtained from the test bundle study, in order to assess the advantages of the proposed formulation.

2. Shell-side fluid flow in shell-and-tube HXCs

The shell-side fluid flow inside shell-and-tube HXCs is particularly complex and it is determined by the simultaneous presence of five mixing and interacting flow streams [12]:

- the main flow stream across the bundle;
- the leakage through tubes-to-baffle clearances;
- the flow bypass between the outermost tubes and the inner shell diameter;
- the baffle-to-shell clearance leakages;
- the flow through any channel within the bundle induced by the presence of pass dividers.

The fluid distribution among these five streams is determined by the relative hydraulic resistances of each one of these paths. Therefore, the correct evaluation of the tube bundle friction factor is of the utmost importance both to assess the overall pressure drop of the equipment and to correctly quantify the occurring bypass phenomena, ultimately responsible for a reduction of the HXC heat transfer performance. Among the several experimental correlations available in the literature for shell-side pressure drop in HXCs, Zukauskas' results are considered here [13]. The pressure drop inside a tube bundle can be evaluated by means of the dimensionless Euler number Eu (equivalent to a friction factor per unit row of tubes), defined as

$$Eu = \frac{\Delta p}{\frac{1}{2} N_{rows} \rho v_{max}^2} \tag{1}$$

where Δp is the total pressure drop, N_{rows} is the number of tube rows crossed by the flow, ρ is the fluid density and v_{max} its maximum velocity, calculated at the minimum bundle cross-section. By considering dimensional analysis arguments, Eu can be expressed as a function of Reynolds number Re and few geometrical parameters, i.e. pitch-over-diameter ratios for in-line and transverse directions. Experimental curves of Eu as a function of Re are available, for different bundle geometries both for in-line and staggered tube arrangements, either in graphical [13] and analytical [1] forms.

The adoption of Zukauskas' correlation inside the porous media model needs an additional manipulation: the velocity magnitude required for both Eu and Re numbers is evaluated at the minimum bundle cross-section "seen" by the moving fluid, and it is dependent on the flow main direction. It is thus necessary to re-define both Eu and Re as a function of the superficial velocity, i.e. the average velocity that would occur if the tubes were removed, simply employing geometrical considerations. The superficial velocity formulation enables the definition of a simple $Eu_s = f(Re_s)$ expression that can be adopted inside the porous media approach with no need to consider the bundle porosity and its direction-dependent permeabilities.

3. HXC inlet section 2D-CFD simulation

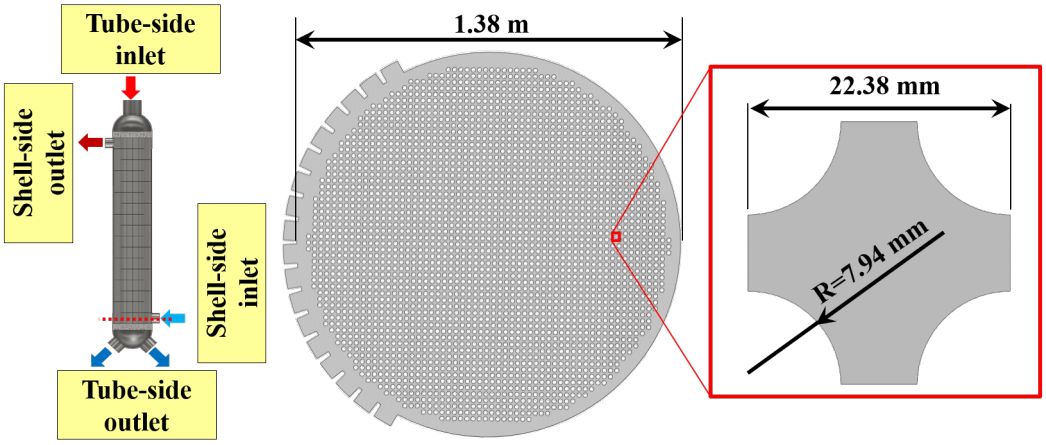

Figure 1. HXC complete geometry (left), 2D inlet section (center) and bundle elementary cell details (right).

The HXC considered for the following simulations is a smaller and simplified version of the DEMO fusion reactor Helium-Molten Salt Intermediate Heat Exchanger (IHX) [14]. With respect to the original DEMO IHX design, the inner shell diameter was roughly halved (from 2.70 to 1.38 m) with the aim to reduce the overall number of tubes (from 10903 to 2643), so to make the simulation manageable with the available computational resources. The details of the resulting geometry are represented in fig. 1. Moreover, the geometry was further simplified, as visible in fig. 2: only half domain was simulated for symmetry reasons, while the tube bundle was cut in correspondence to the baffle plate windows, where the main flow is expected to move along the HXC axial direction. The resulting total number of tubes considered amounts to 1204.

The analyses were performed adopting the Boundary Conditions (BC) shown in fig. 2, while the main assumption and the coolant operating conditions are reported in table 1. Regarding turbulence, ANSYS Generalized $k-\omega$ (GEKO) [11] model with a hybrid wall-function/low-Reynolds wall treatment was adopted.

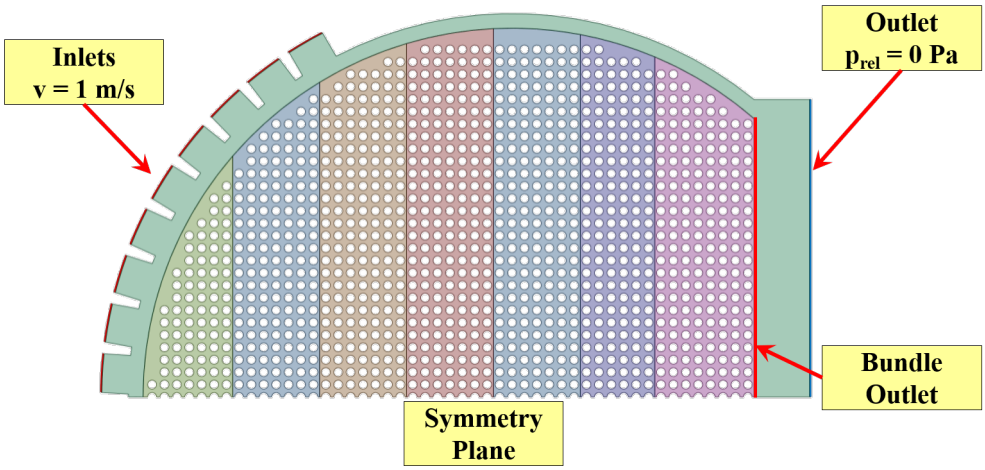

Figure 2. 2D-HXC calculation domain with adopted BCs.

Table 1. Summary of CFD analysis setup.

	Reference Conditions
Analysis Type	Steady-state isothermal
Material Library	Water
Density ρ [kg/m^3]	997
Dynamic Viscosity μ [Pa s]	$8.9{\cdot}10^{-4}$
Turbulence Model	GEKO
Boundary Layer Modelling	Automatic Wall Functions

Some details of the adopted mesh are depicted in fig. 3, while its main parameters and the quality metrics that are most relevant to ANSYS CFX are summarized in table 2. It is worth mentioning that the average mesh quality metrics are within the acceptable ranges prescribed in [11], and only a small fraction ($< 1\%$) of the overall number of cells is characterized by poor quality. Consequently, the results are not expected to be significantly influenced by mesh quality. Moreover, the grid first layer thickness was chosen so to guarantee y^+ values of $\approx$1.

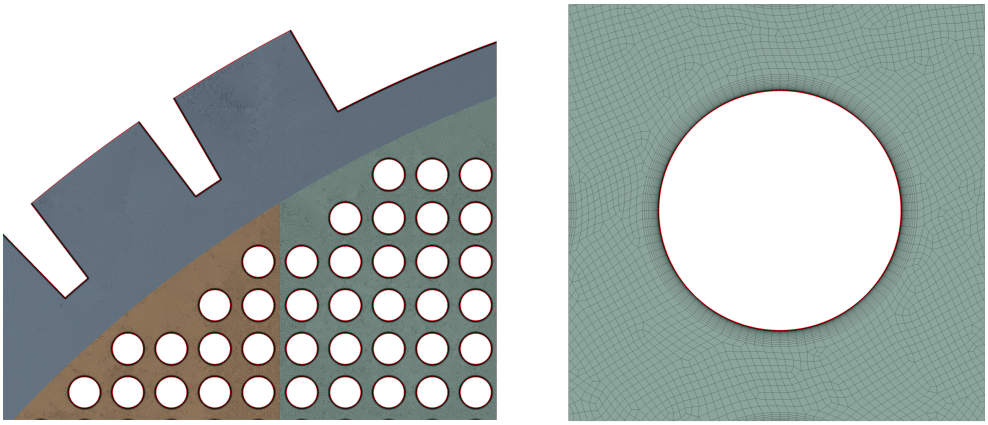

Figure 3. Details of the mesh adopted for the 2D-HXC calculation.

Table 2. Summary of the HXC main mesh parameters and quality metrics.

Mesh Parameter	**Value**
Nodes/Elements	$5.5{\cdot}10^6/5.4{\cdot}10^6$
Elements Topology	Hybrid (Hexa/Prism)
Inflation Layers Number	30
First Layer Thickness [μm]	2
Layers Growth Rate	1.15
Maximum Element Size [mm]	0.50
Mesh Metric	**Value**
Orthogonality Factor (average/min)	0.99/0.07
Expansion Factor (average/max)	1.1/4.5
Aspect Ratio (average/max)	36/247

Two different figures of merit (FoMs) were selected to assess the HXC performance: the total pressure drop and the bypass flow rate, defined as

$$f_{bypass} = 1 - \frac{\dot{m}_{BundleOutlet}}{\dot{m}_{Outlet}} \tag{2}$$

where the mass flow rates are calculated at the Outlet and Bundle Outlet locations as by fig. 2.

The velocity field inside the HXC is reported in fig. 4, while a total pressure drop of 33.7 kPa and a bypass factor of ≈22% were calculated. It is moreover interesting to observe in fig. 4 that the fluid is partially expelled from the tube bundle in the region circled in red, with a consequent increase of the bypass flow.

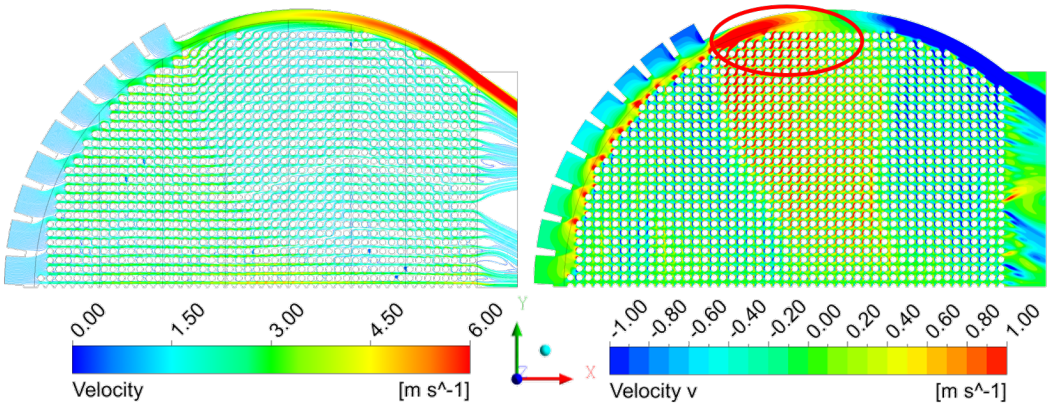

Figure 4. Velocity streamlines (left) and transverse flow velocity (right).

4. 2D-CFD Test Bundle Characterization

The elementary cell of the HXC described in section 3 (visible in fig. 5) was adopted as test bundle, to numerically evaluate the relations between Eu_s and Re_s at different main flow directions by means of 2D-CFD steady-state isothermal analyses, under the same coolant operating conditions of table 1.

With reference to fig. 6, several simulations were performed, imposing the main flow velocity magnitude and direction α. From the analysis of the results obtained, $-\nabla p$ magnitude and direction β were collected, providing a complete map of the test bundle hydraulic resistances. The selection of suitable BCs to be adopted for the simulation resulted challenging, due to the need to precisely control the main flow velocity direction while providing periodic BCs for the Left/Right and Top/Bottom couples of boundaries. The problem was overcome by adopting

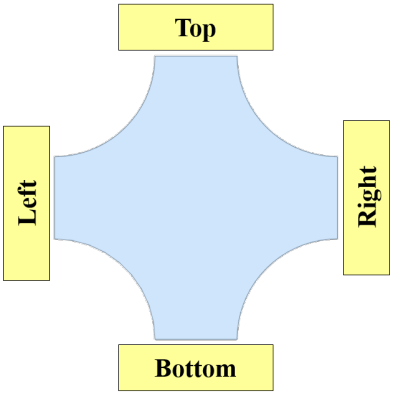

Figure 5. Test bundle geometry and boundary nomenclature.

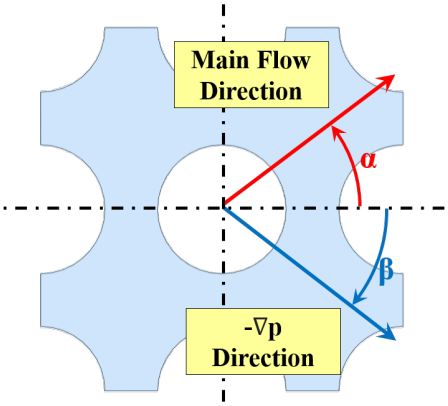

Figure 6. Main velocity and pressure gradient directions with respect to the bundle lattice.

Specified Mass Flow Rate periodic interface conditions (ICs). With this IC model, the solver implements the specified mass flow condition by adjusting the pressure change until the specified mass flow rate is satisfied. Adopting this approach, it is therefore possible to define a specified velocity magnitude taking advantage of the flow incompressibility.

The numerical campaign was conducted considering α values ranging between 0 and 45° at different Re_s values. The results obtained were extended to the range -180 to 180°, exploiting the tube bundle lattice symmetries, and the resulting curves are reported in fig. 7 and fig. 8.

As it may be argued from fig. 7, Eu_s exhibits a quite complex behaviour, characterized by many local minima. At higher values of Re_s, the variations of Eu_s are smaller and the curves tend to flatter. Moreover, it can be observed how the minimum pressure drop is obtained for $\alpha = 45°$ when Re_s is higher than ≈2000, and for $\alpha = 0°$ for lower Re_s numbers. Furthermore, it is interesting to notice in fig. 8 that the pressure gradient is not aligned with the main flow direction.

In particular, β exhibits a pronounced sawtooth shape for high Re_s values, while below $Re_s \approx 4000$, it becomes fairly independent on α.

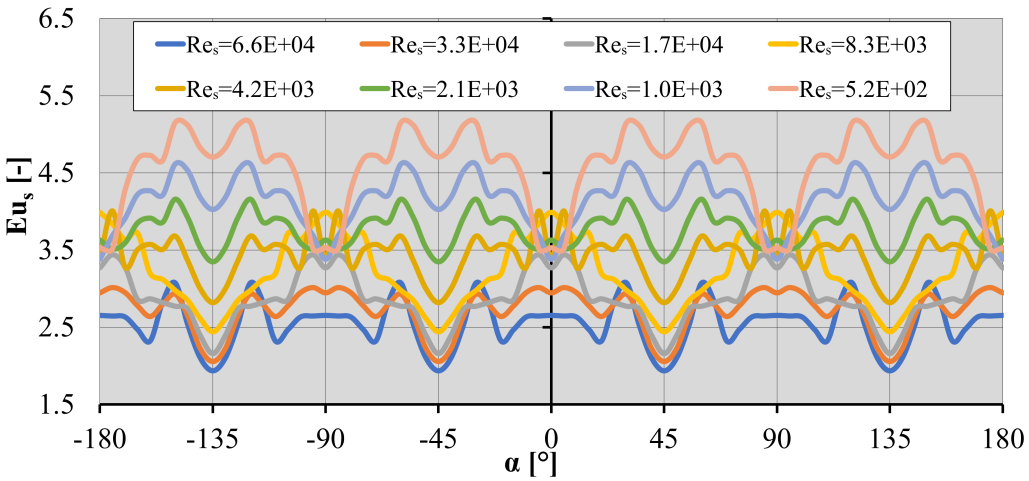

Figure 7. Eu_s as a function of the main flow velocity direction for different Re_s values.

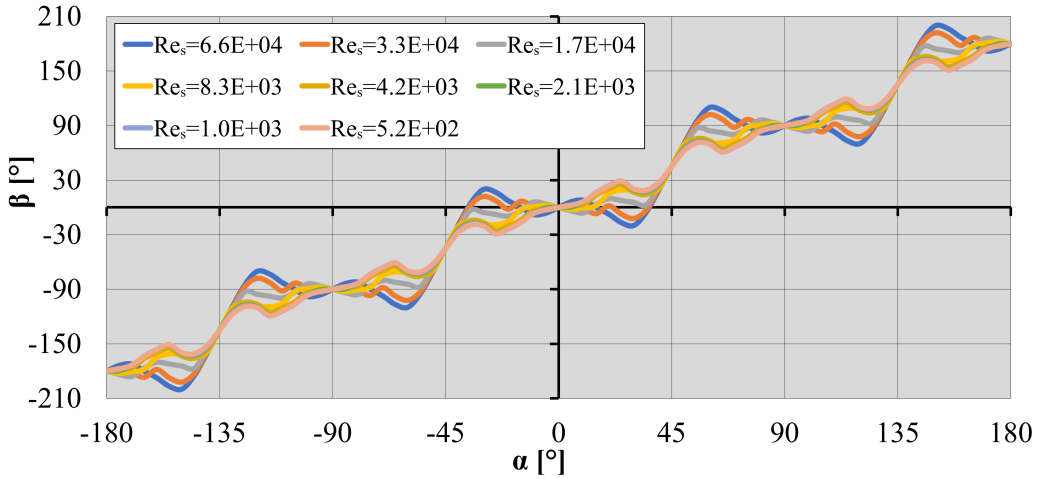

Figure 8. β as a function of the main flow velocity direction for different Re_s values.

Additionally, the results obtained for α=0° and 45° were compared with Zukauskas' experimental curves rescaled according to the superficial velocity formulation, respectively for in-line and staggered tube bundles, as visible in fig. 9. From the analysis of the results obtained, it can be argued that the CFD simulations are able to predict with a good accuracy the experimental results for $Re_s > 10^4$. For Eu_s outside this range, the agreement with experimental data is worse, probably due to turbulence modelling limitations or the assumption of 2D flow, with errors below 30%.

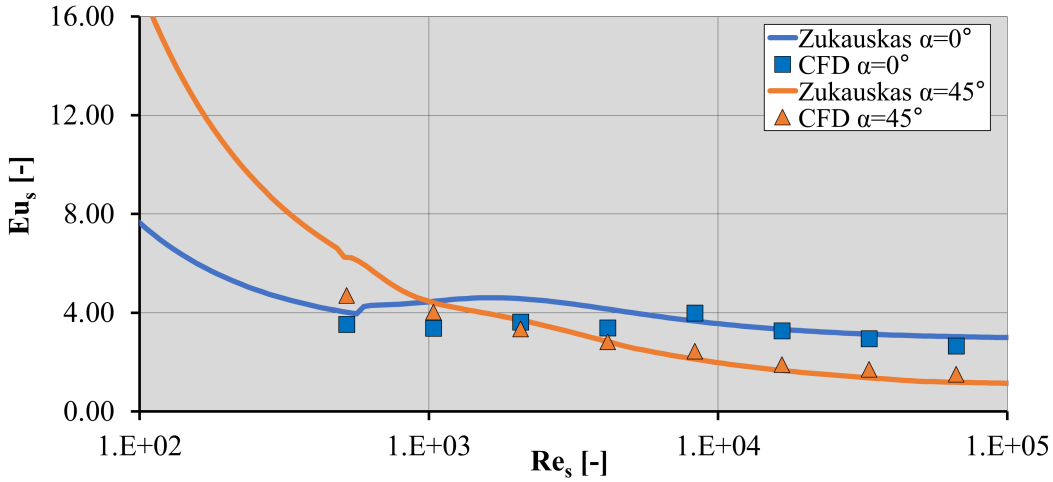

Figure 9. Comparison between Zukauskas' correlation and CFD results.

5. Porous media approach HXC 2D-CFD simulation

The 2D inlet section of the HXC of section 3 was simulated adopting the porous media approach under the same BCs and coolant operating conditions. The geometry was greatly simplified by replacing the tube bundle with a full porous medium, allowing a reduction of the mesh size (whose details are summarized in table 3) by a factor of ≈100, with a consequent remarkable decrease of the computational cost by a factor of ≈20. The momentum sink term was provided starting from the complete maps of Eu_s and β of fig. 7 and fig. 8, supplied in tabular format to the code. It is worth noticing how the reduction of the computational cost related to the lower number of cells is partly lost due to the necessity to interpolate the provided tabular data.

Table 3. Summary of the porous media HXC main mesh parameters and quality metrics.

Mesh Parameter	**Value**
Nodes/Elements	$5.8{\cdot}10^4/5.6{\cdot}10^4$
Elements Topology	Hybrid (Hexa/Prism)
Inflation Layers Number	30
First Layer Thickness [μm]	10
Layers Growth Rate	1.15
Maximum Element Size [mm]	10 (inside bundle region)
Mesh Metric	**Value**
Orthogonality Factor (average/min)	0.95/0.04
Expansion Factor (average/max)	1.1/84.0
Aspect Ratio (average/max)	36/452

The velocity field inside the HXC is reported in fig. 10, showing a good qualitative agreement with the results of section 3. Regarding the two FoMs, the calculated total pressure drop amounts to 35.7 kPa (+6% with respect to the results of section 3), while the bypass factor is ≈20% (against ≈22%).

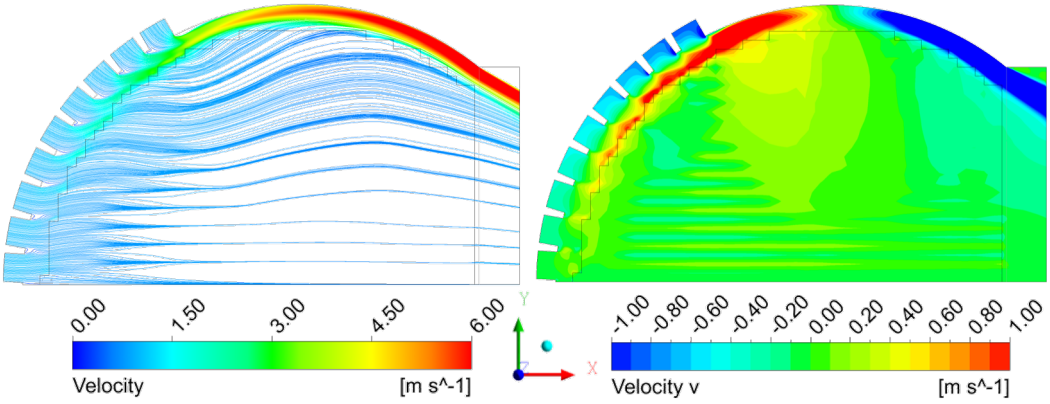

Figure 10. Velocity streamlines (left) and transverse flow velocity (right).

Additionally, to provide a comparison with the existing porous media approaches, the same geometry was tested directly implementing Eu_s from Zukauskas' correlation, following the methodology proposed in [10]. The simulation, whose details are not reported here for the sake of brevity, gave a slightly better prediction of the pressure drop (35.2 kPa, +4%), but considerably underpredicted the bypass flow (≈ 16.7% bypass). The greater bypass factor error may be related to the impossibility of the classical porous medium approach to predict the occurrence of the $\beta = 45°$ low-pressure drop direction at high Re_s, that contributes to the partial flow expulsion from the bundle.

6. Conclusions

A novel numerical methodology to estimate the crossflow shell-side pressure drop has been presented in this paper. To provide a realistic and direction-dependent formulation of the porous media approach, a numerical campaign was performed to study the hydraulic response of a small test bundle at different flow velocity magnitudes and directions. The novel approach was validated with a numerical benchmark, showing a good agreement in terms of pressure drop and bypass prediction. In particular, regarding this latter FoM, the novel methodology indicated better results if compared to the classical porous media formulations.

Disclaimer
This work has been carried out within the framework of the EUROfusion Consortium and has received funding from the Euratom research and training programme 2014-2018 and 2019-2020 under grant agreement No 633053. The views and opinions expressed herein do not necessarily reflect those of the European Commission.

References

[1] E. U. Schlunder, Handbook of Heat Exchager Design, Hemisphere Publishing, 1983.
[2] K. Bell, Delaware method for shell side design, in: S. Kakaç, A. Bergles, F. Mayinger (Eds.), Heat Exchangers: Thermal-Hydraulic Fundamentals and Design, Hemisphere Publishing Corporation, 1981.
[3] E. Ozden, I. Tari, Shell side cfd analysis of a small shell-and-tube heat exchanger, Energy Conversion and Management 51 (5) (2010) 1004–1014.
[4] Q. Wang, et al., Numerical investigation on combined multiple shell-pass shell-and-tube heat exchanger with continuous helical baffles, International Journal of Heat and Mass Transfer 52 (5) (2009) 1214–1222.
[5] J.-F. Zhang, et al., 3d numerical simulation on shell-and-tube heat exchangers with middle-overlapped helical baffles and continuous baffles – part i: Numerical model and results of whole heat exchanger with middle-overlapped helical baffles, International Journal of Heat and Mass Transfer 52 (23) (2009) 5371–5380.
[6] S. Patankar, D. Spalding, Computer analysis of the three-dimensional flow and heat transfer in a steam generator, Numerical Prediction of Flow, Heat Transfer, Turbulence and Combustion (1983) 293–298.
[7] M. Prithiviraj, M. J. Andrews, Three dimensional numerical simulation of shell-and-tube heat exchangers. part i: Foundation and fluid mechanics, Numerical Heat Transfer, Part A: Applications 33 (8) (1998) 799–816.
[8] W. T. Sha, ae al., Multidimensional Numerical Modeling of Heat Exchangers, Journal of Heat Transfer 104 (3) (1982) 417–425.
[9] C. Zhang, et al., Numerical Simulation of Different Types of Steam Surface Condensers, Journal of Energy Resources Technology 113 (2) (1991) 63–70.
[10] Y. He, et al., Numerical simulation and experimental study of flow and heat transfer characteristics of shell side fluid in shell-and-tube heat exchangers, che2005-05, in: Enhanced, Compact and Ultra Compact Heat Exchangers: Science, Engineering and Technology, Hemisphere Publishing Corporation, 2005.
[11] ANSYS Inc., ANSYS CFX-Solver Theory Guide, 2020, Release: 2020 R2.
[12] S. Kakaç, H. Liu, Heat exchangers: Selection, rating, and thermal design, second edition, CRC Press, 2002.
[13] A. Žukauskas, Heat Transfer from Tubes in Crossflow, Advances in Heat Transfer 8 (1972) 93–160.
[14] I. Moscato, Thermal-hydraulic study in support of the design of the DEMO Balance of Plant, Ph.D. thesis, Department of Engineering, University of Palermo, Handle: http://hdl.handle.net/10447/395492 (2020).